ELSEVIER

Tectonophysics 358 (2002) 175–185

TECTONOPHYSICS

www.elsevier.com/locate/tecto

Mapping the lithosphere–asthenosphere boundary through changes in surface-wave anisotropy

Jaroslava Plomerová *, Daniel Kouba, Vladislav Babuška

Geophysical Institute, Czech Academy of Sciences, Boční II, 14131 Prague 4, Czech Republic

Received 20 September 2000; received in revised form 14 May 2001; accepted 15 June 2002

Abstract

The alignment of olivine crystals is considered as the dominant source of seismic anisotropy in the subcrustal lithosphere and asthenosphere. Different components of large-scale anisotropy can be traced in depth distributions of the radial and azimuthal anisotropy of surface waves. We propose a global model of the lithosphere–asthenosphere boundary (LAB) as a transition between a 'frozen-in' anisotropy in the lithosphere to anisotropy in the sublithospheric mantle related to the present-day flow. Due to different orientations of velocity maxima in the anisotropic subcrustal lithosphere and the asthenosphere, the velocity contrast related to the LAB can increase in particular directions. Because of their long wavelengths and horizontal propagation, surface waves suffer from poor lateral resolution. However, surface waves with various wavelengths allow us to map gross features of the LAB with a good vertical resolution. We estimate depths to the LAB to be between 200 and 250 km for the Precambrian shields and platforms, around 100 km for the Phanerozoic continental regions and 40–70 km beneath oceans from the world-wide depth distribution of the radial and azimuthal anisotropy of surface waves.

Keywords: Lithosphere–asthenosphere boundary; Surface waves; Polarisation (radial); Azimuthal anisotropy

1. Introduction

There are various geophysical definitions of the Earth's lithosphere. The lithosphere can be defined as the cold outer shell of the Earth, which can support stress elastically (Anderson, 1989). Alternatively, it is the crust and a part of the upper mantle that translates coherently in the course of plate tectonics (Isaacs et al., 1968). Third, it is a layer in which density and other mechanical properties are controlled by chemical composition and temperature (Jordan, 1978, 1988; Poudjom Djomani et al., 2001). The widely adopted thermal definition considers the lithosphere as a conductive layer above a convecting mantle and associates the lithosphere–asthenosphere boundary (LAB) with an isotherm of about 1300 °C (Artemieva and Mooney, 2002). The LAB is also associated with a layer of increased electrical conductivity caused by partial melting (Jones, 1982). Various physical parameters need not necessarily describe the same boundary. However, several studies demonstrate an agreement

* Corresponding author. Tel.: +420-2-72762279; fax: +420-2-72761549.

E-mail address: jpl@ig.cas.cz (J. Plomerová).

0040-1951/02/$ - see front matter © 2002 Elsevier Science B.V. All rights reserved.
PII: S0040-1951(02)00423-7

between the lithospheric thickness as derived from seismological, thermal and electromagnetic observations (Anderson, 1989; Praus et al., 1990; Babuška and Plomerová, 1993).

Seismology finally defines the lithosphere as the high-velocity outer layer of the Earth, which is at many places underlain by the low-velocity zone (LVZ), a region of diminished velocity or negative velocity gradient in the upper mantle (Gutenberg, 1959). From this and isostatic studies, it has been concluded that a weak region underlies the relatively strong lithosphere. As a consequence, it has been called the asthenosphere. As several physical parameters change at the bottom boundary of the lithosphere, it appears to be one of the most significant discontinuities in the seismic stratification of the upper mantle (Gaherty et al., 1999). The seismic definition describes the LAB from the point of view of mean isotropic velocities. However, since the 1960s, an incompatibility of Love- and Rayleigh-wave dispersion has been found in several studies (Anderson and Harkrider, 1962; Aki and Kaminuma, 1963; Anderson and Toksoz, 1993). The incompatibility between isotropic shear velocities inferred from Love and Rayleigh waves is generally considered a strong diagnostic for the presence of anisotropy in the upper mantle. During the last decade, several studies, based on surface-wave inversions and shear body-wave splitting, have focused on the modelling of seismic anisotropy (Silver, 1996; Montagner, 1998; Debayle and Kennett, 2000). It has been generally accepted that the uppermost mantle is anisotropic from the point of view of propagation of seismic waves (Anderson, 1989; Babuška and Cara, 1991). Montagner and Tanimoto (1991) found that about 2% anisotropy is required in their global 1D anisotropic model of the Earth down to a depth of 200 km. Both surface- and body-wave studies show that strong shear anisotropy is restricted to the upper 200–300 km (e.g., Leveque and Cara, 1983; Gaherty et al., 1999). A two-layered anisotropic model (Debayle and Kennett, 2000) is constrained by the azimuthal anisotropy of SV waves. In the upper layer (down to about 150 km), the anisotropy is related to past deformation frozen in the lithosphere and in the lower layer it reflects present-day deformation due to plate motion. Seismic velocity anisotropy is defined as $k_P = 100(v_P^{max} - v_P^{min})/v_P^{mean}$ (%) for longitudinal P-waves and similarly for shear waves (k_S). Values of k_P about 6–9% and k_S about 4% were found in several regional studies of lithospheric anisotropy based on body waves and xenoliths (Babuška et al., 1984; Mainprice and Silver, 1993; see also Silver, 1996; Savage, 1999 for reviews of shear-wave anisotropy).

Characteristics of the upper mantle anisotropy change both vertically and laterally. In the continental mantle lithosphere, we observe dipping orientation of the high-velocity directions which are consistent within individual lithospheric domains (Babuška et al., 1993; Plomerová et al., 1996, 2000, 2001; Levin et al., 1996; Houseman et al., 2001). Distinct and abrupt changes in 3D orientation of anisotropy often relate to prominent tectonic boundaries between individual lithospheric domains, which have been assembled during a continental accretion. Individual continental domains of the lithosphere have different histories, tectonic development and origin. Therefore, a ‘frozen-in’ origin of seismic anisotropy in the continental mantle lithosphere is the most plausible explanation rather than being formed by the stress field due to the present-day plate motion (Savage, 1999). The structure of the oceanic lithosphere seems to be simpler. The high velocities due to the lattice-preferred orientation (LPO) of olivine are subhorizontal and aligned approximately parallel to the ancient sea-floor spreading (Nicolas and Christensen, 1987; Barruol et al., 1997).

In the sublithospheric part of the upper mantle, both beneath continents and oceans, the high-velocity directions are explained by the *a*-axes of olivine crystals oriented parallel to a present-day flow. The upper mantle flow is prevailingly subhorizontal in a global scale, with several local ascending or descending currents (Montagner, 1994). Similarly, according to orientation of anisotropy, one can model a generally oriented, dipping anisotropy in the continental lithosphere and a subhorizontal anisotropy in the sublithospheric mantle. If it is so, a boundary between the two anisotropic layers should exist in the upper mantle (Gaherty and Jordan, 1995). Therefore, besides a difference in the thermal state of the lithosphere and asthenosphere, and in isotropic seismic velocities, a change in seismic anisotropy may be distinctive for the LAB. Due to seismic anisotropy, the velocity contrast related to this boundary can be much larger

than that which could be produced by compositional variations and thermal state alone (Babuška and Cara, 1991; Sobolev et al., 1997).

The Lehmann discontinuity (L) was originally associated with the lower boundary of the asthenospheric LVZ (Lehmann, 1961) or with the top of a region of high-velocity gradient between 250 and 350 km depth. Later, it was proposed as a discontinuity separating anisotropic layers in the upper mantle at average depth of 220 km world-wide (Leven et al., 1981; Revenaugh and Jordan, 1991; Karato, 1992; see also Gaherty and Jordan, 1995 for a review). Savage (1999) considers L as a possible boundary between "'frozen-in' past anisotropy and present strain."

In this paper, we propose a model for the discontinuity between the 'frozen-in' seismic anisotropy and the anisotropy due to present-day flow in the upper mantle. The discontinuity is mapped through changes of depth-dependence of relative polarisation anisotropy (ξ_R), formerly also called radial anisotropy, and azimuthal ($\boldsymbol{G}$) anisotropy of surface waves (Montagner, 1994; Babuška et al., 1998). We associate depths of the transition between the fossile seismic anisotropy and the anisotropy due to present-day flow with depths of the LAB.

2. Mapping changes in the upper mantle anisotropy

Surface-wave anisotropy, which relates to S-wave anisotropy, is determined by the two parameters of anisotropy, ξ and G, depending on elastic coefficients (c_{ij}), as well as on velocities. The polarisation anisotropy is defined as $\xi=(N-L)/L \approx 2(v_{SH}-v_{SV})/v_{SV}$, where $N=\rho v_{SH}^2 = 1/8(c_{11}+c_{22}) - 1/4(c_{12}) + 1/2(c_{66})$ and $L=\rho v_{SV}^2 = 1/2(c_{44}+c_{55})$, and where ρ stands for density. The ξ expresses differences between the horizontal (v_{SH}) and vertical (v_{SV}) shear velocities. The polarisation anisotropy ξ can be related to the orientation of olivine crystals and/or to the type of flow in the mantle. Basically, ξ tends to be positive for a subhorizontal flow and negative for a vertical flow. The azimuthal anisotropy $\boldsymbol{G}(G, \psi_G)$ expresses azimuthal variations of v_{SV} (Montagner and Nataf, 1986) and it is described by cos $G_c=(c_{55}-c_{44})/2$ and sin $G_s=c_{54}$ terms. The azimuthal anisotropy exhibits π periodicity and is given by amplitude G and azimuth ψ_G, denoting azimuth along a wave path.

Babuška et al. (1998) studied the depth distribution of the relative polarisation anisotropy $\xi_R=\xi-\xi_0$, where ξ_0 is for a model anisotropy. Here, the 1D anisotropic model ACY400 was used for ξ_0 (Montagner and Tanimoto, 1991). The upper 200 km of this radial reference model based on surface-wave data is characterised by 2% polarisation anisotropy, which decreases below this depth down to 400 km. Below 400 km, the model is isotropic. The anisotropic parameters of the global 3D upper mantle model (AUM) are given as a $10\times10^\circ$ grid down to 500 km depth, with a vertical resolution of about 50 km down to 200 km depth, with an error of less than 1%. Resolution decreases with increasing depth. The perturbations from the model, ξ_R, are approximately $\pm5\%$ within the upper 150 km. Simons et al. (1999) found that lithosphere shear-wave speed, derived from Rayleigh waves recorded at a dense portable array in Australia (van der Hilst et al., 1998), varies as much within domains of similar crustal age as between units of different ages. Nevertheless, considering both the polarisation and azimuthal anisotropy of Love and Rayleigh waves allowed us to infer an age-dependent large-scale fabric in the mantle lithosphere. Original manual standardisation of depth-dependence of ξ_R for the North American and Eurasian continents (Babuška et al., 1998) was automated in this paper and extended to the global data.

Depth distributions of relative polarisation anisotropy ξ_R in a $10\times10^\circ$ grid can be divided into five main groups according to their specific depth-dependence in the upper 200 km (Fig. 1). Two of the types, marked as Types 1 and 4, exhibit negative deviations in the uppermost mantle (specifically between 45 and 80 km) relative to model ACY400. While the ξ_R decreases in this depth interval and reaches a minimum at depth about 100 km, the ξ_R of Type 4 increases from negative to positive values with depth. Other two types, Types 3 and 2, exhibit distinct positive deviations. Type 3 is characterised by either a monotonous decrease of ξ_R with depth below about 70 km, or, it exhibits a minimum at depth below 200 km (triangles and dots in Fig. 1, respectively). ξ_R of Type 2 shows a minimum at depth above 200 km. Type 5 does not show clear negative or positive deviations from the reference model and varies with depth within a $\pm0.5\%$ limit relative to its mean value in the upper 150 km.

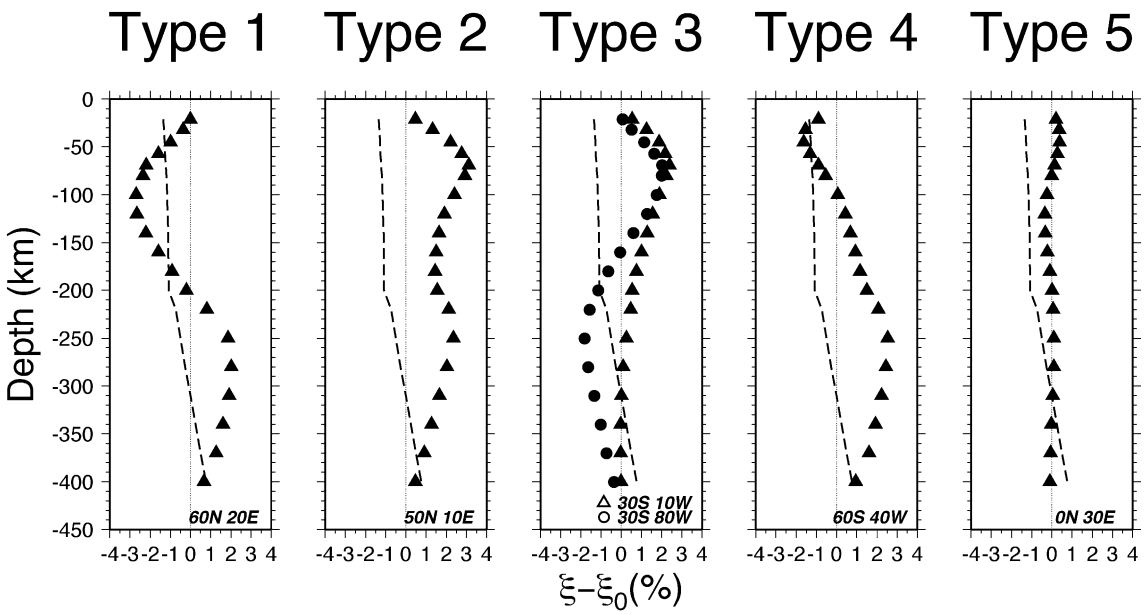

Fig. 1. Examples of five types of the specific depth-dependence of the relative polarisation anisotropy $\xi_R = \xi - \xi_0$ (dashed line marks $-\xi_0$). The polarisation anisotropy ξ measures the difference between the horizontal and vertical shear-wave velocities. Types 1, 2 and 3 are mostly observed in Precambrian, Phanerozoic and oceanic regions, respectively. Type 4 represents transitional regions and Type 5 regions with minimum deviation from the 1D model. Parameters of the surface-wave anisotropy (ξ and $\boldsymbol{G}$) were extracted from the global 3D anisotropic model AUM and ξ_0 is the reference 1D anisotropic model ACY400 (Montagner and Tanimoto, 1991).

Lateral variations of the type are systematic and indicate regions with similar ξ_R (Fig. 2). However, there is a subtle difference between Types 2 and 3, corresponding to orogenic and oceanic lithosphere (see below). In some regions of northern Africa or western North America, the depth distributions are very similar at around 200 km depth. On the other hand, world-wide comparison of the polarisation anisotropy ξ_R in the mantle lithosphere, at a scale $10 \times 10^\circ$, correlates to a certain degree (Babuška et al., 1998) with the age of continental provinces (e.g., Zandt and Ammon, 1995; Kusky and Polat, 1999) and types of the Earth's crust (Mooney et al., 1998). The surface-wave anisotropy beneath Precambrian shields and platforms is characterised mostly by negative ξ_R (mostly Type 1, see Fig. 1), indicating that $v_{SV} \sim v_{SH}$ or even $v_{SV} \geq v_{SH}$ at some depths. Due to the fact that the five types of characteristic depth distribution of polarisation anisotropy ξ_R are ascribed to $10 \times 10^\circ$ intersections, they represent a very large volume of the mantle lithosphere. Therefore, relatively small size features of crustal tectonics, e.g., narrow orogenic belts surrounded by large Precambrian units, are not reflected in the map of types in Fig. 2.

The maximum perturbation of the relative polarisation anisotropy is at depths of about 100 km (Babuška et al., 1998). In western Australia, the specific depth-dependence of ξ_R is of Type 1 with values larger than -2%, while the minima of ξ_R commonly found in Precambrian regions attain -5%. This means that v_{SH} is comparable with v_{SV}, or it remains larger than v_{SV} beneath the Australian continent. This is in agreement with results of the surface wave tomography (Debayle and Kennett, 2000). On the other hand, beneath Phanerozoic regions and beneath oceans, ξ_R is positive, reflecting that $v_{SH} > v_{SV}$. Though the types are ascribed to the intersections of the $10 \times 10^\circ$ cells, due to the long wavelength of the surface waves, the dependence represents a relatively large volume of the upper mantle, which extends with increasing depth.

The polarisation anisotropy ξ provides information regarding the ratio of v_{SV}/v_{SH}, while the depth distribution of azimuthal anisotropy $\boldsymbol{G}$ shows variations in amplitude and orientation of v_{SV}. Several compo-

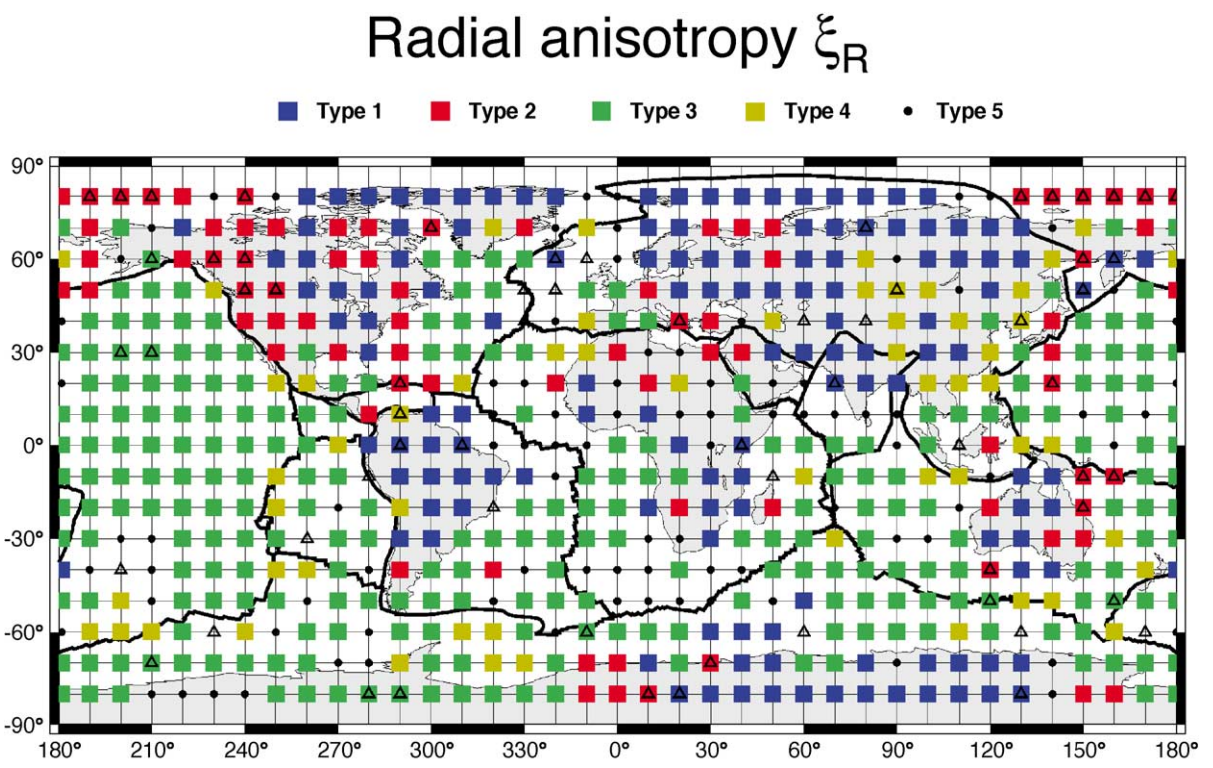

Fig. 2. World-wide distribution of the five types of $\xi_R(h)$ specified in Fig. 1 and shown for $10 \times 10°$ grid. The triangles mark intersections where the depth-dependence of ξ_R could not be assigned to any of the five types or were checked manually (9% of the total number).

nents can be recognised in depth distributions of ***G***, which reflects namely the anisotropy of the crust, the mantle lithosphere and in the sublithospheric mantle. The azimuthal anisotropy differs in amplitudes and in orientation with depth. Usually, the strongest anisotropic signal in ***G*** is observed in the mantle lithosphere beneath the continents, while beneath the oceans, the azimuthal anisotropy in the mantle lithosphere and in the sublithospheric mantle are often comparable (see Fig. 3c). The relatively strong signal of ***G*** beneath the oceanic plates is most likely related to the well-developed asthenospheric LVZ beneath the oceans, with its upper boundary denoted as the Gutenberg discontinuity (Revenaugh and Jordan, 1991). The weakest sublithospheric signal of azimuthal anisotropy is found beneath stable Precambrian cratons.

We inspect the characteristics of the depth distributions of polarisation anisotropy ξ_R and azimuthal anisotropy $\boldsymbol{G}(G, \psi_G)$ to estimate the depth of the transition from the 'frozen-in' anisotropy in the lithosphere to the anisotropy reflecting the 'present-day' flow in the asthenosphere (Silver, 1996; Barruol et al., 1997; Savage, 1999). Assuming the anisotropic signal need not be coherent in the mantle lithosphere and sublithospheric mantle, we look mainly for a change in orientation (ψ_G) and in amplitude (G) of ***G***. The change is located above the extreme of ξ_R, which reflects the present-day mantle flow (Fig. 3). The changes in anisotropy were located automatically as either a distinct change in azimuth ψ_G, or they were estimated from a defined decay in amplitudes for the case of coherently oriented azimuthal anisotropy in both layers (Fig. 3d).

The minimum of ξ_R of Type 1 (Fig. 3a), found mainly in the Precambrian areas with a thick crust (see Fig. 2), marks a depth where $v_{SV} \geq v_{SH}$, indicating a rather steep dip of high-velocity orientation frozen in the lithosphere (Babuška et al., 1998). We note that v_{SV} is absolutely larger than v_{SH} if $\xi_R < -2\%$ at depths shallower than 200 km. Therefore, the discontinuity is

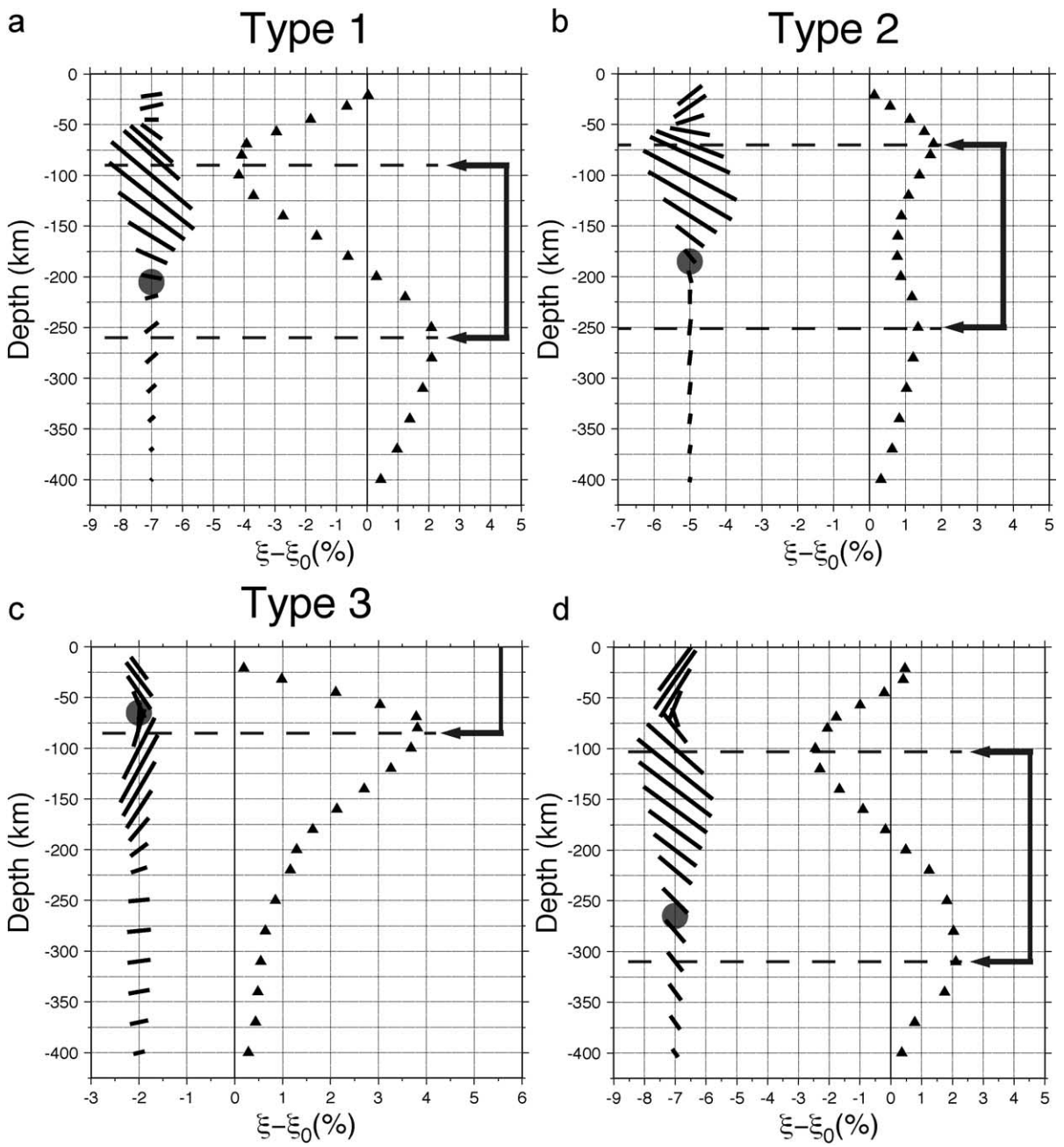

Fig. 3. Determination of depths of a discontinuity in anisotropy (full circle) related to the LAB for three basic types of the depth-dependence of ξ_R (triangles). Changes in orientation (a, b, c), or in amplitudes (d) of the vector $\boldsymbol{G}(G, \psi_G)$, where the magnitude of G is proportional to the length of thick lines in the left-hand side of the figures and azimuth ψ_G is shown clockwise from the vertical, are searched in a depth range (marked by the interconnected arrows) above the $\xi_R(h)$ extreme related to the mantle anisotropy reflecting the present-day flow in the asthenosphere. The olivine lattice-preferred orientation due to a past deformation or a present stress field is responsible for the observed seismic anisotropy of the different origin. The transition is related to the change from the frozen-in anisotropy in the mantle lithosphere to anisotropy caused by a present-day flow beneath the lithosphere.

associated with a change of $\boldsymbol{G}$ at a depth between the minimum and maximum of ξ_R. This maximum marks a region with $v_{SH}>v_{SV}$ related to subhorizontal mantle flow. Similarly, for ξ_R of Type 2 (Fig. 3b), found mainly in orogenic belts, the depth of the transition is again sought between the local extremes; however, the shallower one is in this case positive as compared with a negative shallow extreme for Type 1.We suggest that the upper maximum reflects moderately dipping anisotropic structures frozen in the Phanerozoic continental lithosphere. For Type 3 (Fig. 3c) the oceanic crust is very thin and its anisotropy is not resolved by the long period surface waves. Likewise, the oceanic lithosphere is thinner as compared to that beneath the continents. As a consequence, in the upper mantle beneath the oceans we associate the maximum of ξ_R of Type 3 with the well-developed sublithospheric LVZ.

Besides the three basic types of ξ_R, we observe two other shapes of the depth-dependence. A transitional shape called Type 4, characterised in the depth interval of 45–80 km by an increase of the polarisation anisotropy from negative values (Fig. 1), was found mainly around plate margins and in central and southeast Asia (Fig. 2). At some places, mostly under oceans, perturbations of less than $\pm 0.5\%$ were found; this defines Type 5. For these two types, a depth for the change of $\boldsymbol{G}$ was determined manually taking into account the tectonic environment, as well as the criteria described above.

3. Global model of lithosphere thickness

A proposed global model of the lithosphere thickness, based on the depth-dependence of the relative polarisation anisotropy ξ_R and azimuthal anisotropy $\boldsymbol{G}(G, \psi_G)$ of surface waves, is presented in Fig. 4. There is a correlation between the depth of the LAB and the Earth's tectonics. The thickest lithosphere,

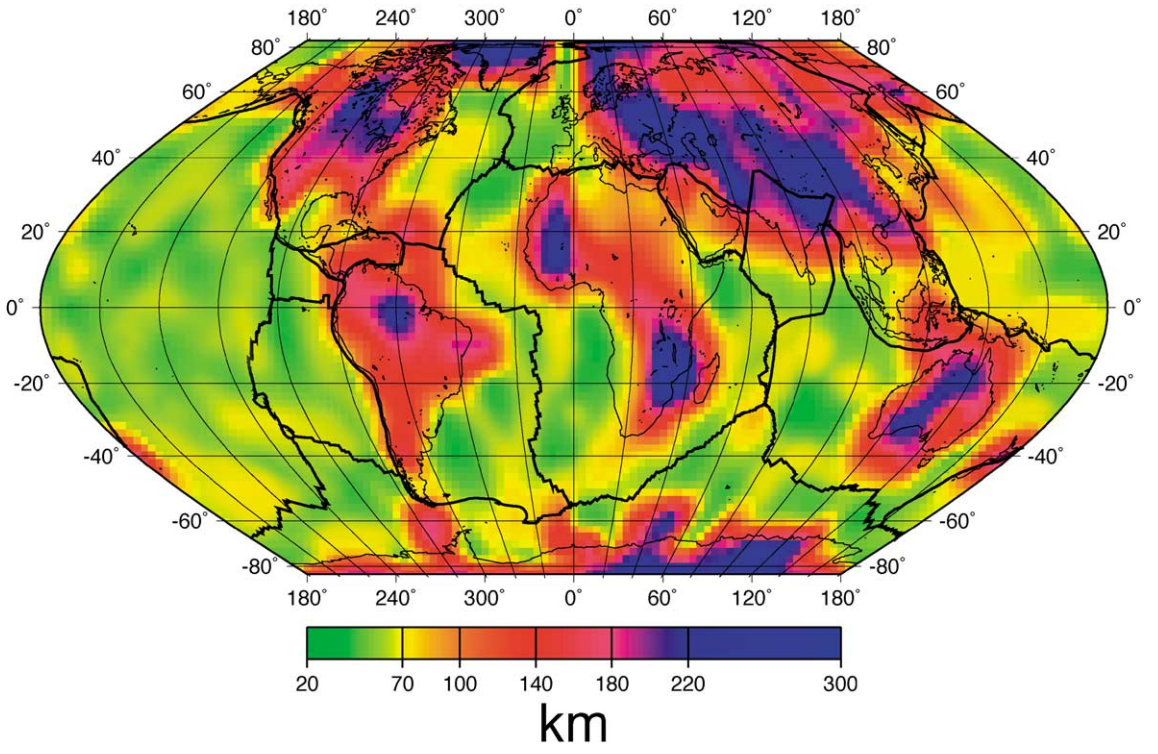

Fig. 4. Proposed global model of the lithosphere–asthenosphere boundary (LAB) defined as a transition between the frozen-in anisotropy in the mantle lithosphere and anisotropy due to a present-day flow in the sublithospheric upper mantle derived from polarisation and azimuthal anisotropy of surface waves.

about 250 km, was found beneath old cratonic areas—the Archean cratons of North America (Canadian Shield) and Greenland, central Brazil, the Kaapwaal and west African cratons, most of Australia, and the Precambrian of Antarctica. The largest region of a thick lithosphere extends from Fennoscandia to the eastern part of the Indian Shield, eastern Siberia and China, though it comprises, besides extensive shields and Precambrian platforms, also several young orogenic belts as the Himalayas and Tibet. On the other hand, we have found a thickness only of about 150–200 km beneath the eastern Siberia, where Artemieva and Mooney (2002) modelled a very thick thermal lithosphere.

As mentioned before, the $10 \times 10^{\circ}$ grid of data allows us to see only gross features of the lithosphere–asthenosphere transition. From this point of view, Europe represents a small, poorly resolved region and the complexity of its tectonics can hardly be detected. However, the proposed model clearly shows the thin Phanerozoic lithosphere to the southwest of the Trans-European Suture Zone (TESZ, Pharaoh, 1999), and the thick lithosphere beneath the Precambrian East European Platform and the Baltic Shield to the northeast of the suture. Surprisingly, vast regions of central Asia with Phanerozoic crust (Mooney et al., 1998) also show signs of a thick lithosphere characteristic of cratonic regions. It is probable that the lithosphere there is substantially thickened due to the collision of India with Asia.

As expected, the thinnest lithosphere is observed beneath the oceans (Fig. 4). In general, the whole Mid-Atlantic Ridge shows a thickening of the oceanic lithosphere in direction of the sea-floor spreading. However, in agreement with Gaherty et al. (1999), our results do not suggest that a pure cooling process can explain thickening of the oceanic lithosphere with age. We also observe a thicker lithosphere in the Philippine Sea ridge environment (10°N 130°E–40°N 140°E), which is younger than the Pacific (20°S 180°E–20°N 200°E), where the lithosphere is thinner (Fig. 4). However, the accuracy of our model, based on data which sample the outer shell of the Earth from 20 km depth with a step of 12 km is low, especially in oceanic regions with a thin crust and lithosphere. In addition, the process of lithosphere thickening from below by a simple cooling cannot explain the dipping structures observed in the continental lithospheric domains.

4. Discussion and conclusions

The study of seismic anisotropy, as a distinct phenomenon of the upper mantle due to preferred orientation of olivine crystals, is a tool to understand the large-scale fabric of the upper mantle (Babuška and Cara, 1991). Various approaches, based on analyses of body waves, reveal dipping anisotropic structures in continental provinces (Babuška et al., 1993; Plomerová et al., 1996; Levin et al., 1996; Frederiksen and Bostock, 2000). A method of constructing three-dimensional (3D) self-consistent anisotropic models (Šílený and Plomerová, 1996) of the continental lithosphere allows us to detect lateral changes of the large-scale fabric of individual lithospheric blocks. The changes occur at boundaries of lithospheric blocks. A concept of anisotropic domains of the mantle lithosphere (Plomerová et al., 1996, 2000) resulted from these findings. Anisotropy of the lithospheric domains is interpreted as having a 'frozen-in' origin (Babuška and Cara, 1991; Savage, 1999; Debayle and Kennett, 2000). A complex and most probably vertically varying anisotropic structure of the lithospheric domains, e.g., beneath Australia (Clitheroe and van der Hilst, 1998; Kennett, 2001), is reflected in laterally varying azimuthal anisotropy derived from the shear-wave splitting. Moreover, Saltzer et al. (2000) showed on synthetics that such structures, represented, e.g., by a two-layered anisotropic medium, can even produce a 'null' splitting despite the fact that waves travelled through a strongly anisotropic medium. Considering only simple one-layered anisotropic model of the upper mantle with horizontal axes can be then interpreted as a discrepancy between anisotropic observations of surface and body waves. Anisotropy produced by shear deformation along prominent sutures (McNamara et al., 1994; Barruol and Souriau, 1995; Vauchez et al., 1998) represents one component of the observed effective anisotropy. Different types and orientations of anisotropic structures, detected by body-wave observations in continental domains are integrated by observations of long-period surface waves.

The analysis of the depth distribution of surface-wave anisotropy (Montagner, 1994) is a challenge.

Large-scale anisotropic structures of the mantle lithosphere can be modelled by olivine (a,c) foliation planes plunging steeply beneath Precambrian shields and platforms, compared with Phanerozoic provinces and oceans, which show moderately dipping (a,c) or subhorizontal foliation (Babuška et al., 1998). Therefore, Mohorovicic, Lehmann and Gutenberg upper mantle discontinuities, originally associated with distinct changes in average seismic velocities, can also be related to changes in seismic anisotropy. In our attempt to model the LAB, we associate its depth with changes in anisotropy due to the difference in its origin. We define the LAB as a transition between a 'frozen-in' anisotropy in the mantle lithosphere and a present-day anisotropy due to a flow in the sublithospheric mantle. The modelling is based on changes of azimuthal $\boldsymbol{G}(G, \psi_G)$ and relative polarisation ξ_R anisotropy of surface waves with depth.

Various estimates of the LAB are based on isotropic seismic velocities (Babuška and Plomerová, 1993), especially in velocity–perturbation tomography studies (Iyer and Hiraharam, 1993; Kennett, 1998). Seismic estimates of the lithospheric thickness have either used the anisotropy as the base for defining the thickness or have ignored it. It is evident that due to the differences in orientation of dipping anisotropic structures (the (a,c) olivine foliation) in the continental subcrustal lithosphere and the asthenosphere, the lithosphere–asthenosphere velocity contrast can increase. Velocity anomalies in the upper mantle are strongly affected by different orientations of dipping anisotropic structures within the mantle lithosphere. Neglecting the seismic anisotropy, which cannot be considered as a second-order effect (Anderson, 1989), increases errors in the LAB estimates based on isotropic velocities. Seismic waves propagating in dipping anisotropic structures can be misinterpreted as having velocities higher than their true average in isotropic studies. This can produce a false high-velocity heterogeneity, e.g., a high-velocity lithospheric slab (Sobolev et al., 1997). In regions with steeply dipping high velocities, the isotropic studies can result in an over estimate of lithosphere thickness.

The thickest continental lithosphere, independent of method used, is found beneath the Precambrian cratonic areas. However, the common thickness of 200–250 km derived from changes of anisotropy (Fig. 4) is smaller than the thickness up to 350–400 km, found in global seismic tomographic studies (e.g., Zhang and Tanimoto, 1993; Grand, 1994). Depths of the lithospheric roots shallower than those from the global models are also reported from regional tomographic studies (Bijwaard et al., 1998; Ritsema and van Heijst, 2000; Debayle and Kennett, 2000) and are supported by thermal estimates (Artemieva and Mooney, 2002). Shallower depths for the LAB are in agreement with models of mantle convection assessing to these depths equilibrium of cratonic roots and a secondary convection (Doin et al., 1997). However, accuracy of intrinsic values—parameters ξ and $\boldsymbol{G}$—with a depth resolution of 50 km, limits the accuracy of the model. Moreover, especially in continental regions, the $10 \times 10^\circ$ grid of data is not sufficient to detect short-wavelength topography at the base of the LAB. Therefore, a more detailed study with a higher density of anisotropic information will be the target of future research.

We conclude that the boundary between the fossile seismic anisotropy and the anisotropy due to present-day flow in the upper mantle determined from changes of depth-dependence of relative polarisation anisotropy (ξ_R) and azimuthal ($\boldsymbol{G}$) anisotropy of surface waves can be associated with the LAB. The proposed global model shows the thickest lithosphere up to 200–250 km beneath Precambrian shields and platforms, as well as beneath several collision zones in Asia; the lithospheric thickness decreases to about 100 km, on average, for the Phanerozoic continental regions, and up to 40–70 km beneath oceans.

Acknowledgements

We thank J.-P. Montagner for providing data on the surface-wave anisotropy and N. Giradin for her cooperation in the preparatory stage of this study. The paper benefited from thorough reviews of two anonymous referees and reviews by G. Bock and G. Chulick. We are also grateful for improvements suggested by one of the guest editors W. Mooney and by the editor-in-chief H. Thybo. All comments substantially improved the manuscript. We used GMT (Wessel and Smith, 1995) to plot the majority of figures in this paper. The research was partly supported by grant no. A3012908 of the Grant Agency of the Czech Academy of Science.

References

Aki, K., Kaminuma, K., 1963. Phase velocity in Japan: Part I. Love waves from the Aleutian shocks of March 9, 1957. Bull. Earthq. Res. Inst. 41, 243–259.

Anderson, D.L., 1989. Theory of the Earth. Blackwell, 366 pp.

Anderson, D.L., Harkrider, D., 1962. The effect of anisotropy on the oceanic lithosphere. Geophys. Res. Lett. 10, 841–844.

Anderson, D.L., Toksoz, M.N., 1993. Upper mantle structure from Love waves. J. Geophys. Res. 68, 3483–3500.

Artemieva, I., Mooney, W., 2002. Thermal thickness and evolution of Precambrian lithosphere: a global study. J. Geophys. Res. 106, 16387–16416.

Babuška, V., Cara, M., 1991. Seismic Anisotropy in the Earth. Kluwer Acad. Publ., Dordrecht, 217 pp.

Babuška, V., Plomerová, J., 1993. Lithosphere thickness and velocity anisotropy—seismological and geothermal aspects. Tectonophysics 225, 79–89.

Babuška, V., Plomerová, J., Šílený, J., 1984. Large-scale oriented structures in the subcrustal lithosphere of central Europe. Ann. Geophys. 2, 649–662.

Babuška, V., Plomerová, J., Šílený, J., 1993. Models of seismic anisotropy in deep continental lithosphere. Phys. Earth Planet. Inter. 78, 167–191.

Babuška, V., Montagner, J.-P., Plomerová, J., Girardin, N., 1998. Age-dependent large-scale fabric of the mantle lithosphere as derived from surface-wave velocity anisotropy. Pure Appl. Geophys. 151, 257–280.

Barruol, G., Souriau, A., 1995. Anisotropy beneath the Pyrenees range from teleseismic shear wave splitting: results from a test experiment. Geophys. Res. Lett. 22, 493–496.

Barruol, G., Helffrich, G., Vauchez, A., 1997. Shear wave splitting around the northern Atlantic: frozen Pangaean lithospheric anisotropy? Tectonophysics 279, 114–135.

Bijwaard, H., Spakman, W., Engdahl, E.R., 1998. Closing the gap between regional and global travel time tomography. J. Geophys. Res. 103 (B12), 30055–30078.

Clitheroe, G., van der Hilst, R., 1998. Complex anisotropy in the Australian lithosphere from shear-wave splitting in broad-band SKS records. In: Braun, J., et al., (Eds.), Structure and Evolution of the Australian Continent. Geodyn. Ser., vol. 26. AGU, Washington, DC, pp. 73–78.

Debayle, E., Kennett, B.L.N., 2000. Anisotropy in the Australasian upper mantle from Love and Rayleigh waveform inversion. Earth Planet. Sci. Lett. 184, 339–351.

Doin, M.-P., Fleitout, L., Christensen, U., 1997. Mantle convection and stability of depleted and undepleted continental lithosphere. J. Geophys. Res. 102, 2771–2787.

Frederiksen, A.W., Bostock, M.G., 2000. Modelling teleseismic waves in dipping anisotropic structures. Geophys. J. Int. 141, 401–412.

Gaherty, J.B., Jordan, T.H., 1995. Lehmann discontinuity as the base of an anisotropic layer beneath continents. Science 268, 1468–1471.

Gaherty, J.B., Kato, M., Jordan, T.H., 1999. Seismological structure of the upper mantle: a regional comparison of seismic layering. Phys. Earth Planet. Inter. 110, 21–41.

Grand, S.P., 1994. Mantle shear structure beneath the Americas and surrounding oceans. J. Geophys. Res. 99 (B6), 11591–11621.

Gutenberg, B., 1959. Physics of the Earth's Interior. Academic Press, New York, 240 pp.

Houseman, G.A., Graeber, F.M., Greenhalgh, S.A., 2001. The three-dimensional seismic structure of the Paleozoic Lachlan Foldbelt of SE Australia. Geophys. Res. Abstr. 3 (EGS).

Isaacs, B., Oliver, J., Sykes, L.R., 1968. Seismology and the new global tectonics. J. Geophys. Res. 73, 5855–5899.

Iyer, H., Hiraharam, K., 1993. Seismic Tomography. Chapmann & Hall, London, 842 pp.

Jones, A.G., 1982. Observations of electrical asthenosphere beneath Scandinavia. Tectonophysics 90, 37–355.

Jordan, T.H., 1978. Composition and development of the continental tectosphere. Nature 274, 544–548.

Jordan, T.H., 1988. Structure and formation of the continental tectosphere. J. Petrol., 11–37 (Special Lithosphere issue).

Karato, S.-I., 1992. On the Lehmann discontinuity. Geophys. Res. Lett. 19, 2255–2258.

Kennett, B.L.N., 1998. Seismic Wave Propagation and Seismic Tomography. The Australian National University, Canberra, 116 pp.

Kennett, B.L.N., 2001. The lithosphere and asthenosphere in the Australian region. IAGA-IASPEI Abstr., 50.

Kusky, T.M., Polat, A., 1999. Growth of granite–greenstone terranes at convergent margins, and stabilization of Archean cratons. Tectonophysics 305, 43–73.

Lehmann, I., 1961. S and the structure of the upper mantle. Geophys. J. R. Astron. Soc. 4, 124–138.

Leven, J.H., Jackson, I., Ringwood, A.E., 1981. Upper mantle seismic anisotropy and lithospheric decoupling. Nature 289, 234–239.

Leveque, J.J., Cara, M., 1983. Long-period love wave overtone data in North America and Pacific Ocean; new evidence for upper mantle anisotropy. Phys. Earth Planet. Inter. 33, 164–179.

Levin, V., Menke, W., Lerner-Lam, A., 1996. Seismic anisotropy in the north-eastern US as a source of significant teleseismic P traveltime anomalies. Geophys. J. Int. 126, 593–603.

Mainprice, D., Silver, P.G., 1993. Interpretation of SKS-waves using samples from the subcontinental lithosphere. Phys. Earth Planet. Inter. 78, 257–280.

McNamara, D.E., Owens, T.J., Silver, P.G., Wu, F.T., 1994. Shear wave anisotropy beneath the Tibetian Plateau. J. Geophys. Res. 99 (B7), 13655–13665.

Montagner, J.-P., 1994. Can seismology tell us anything about convection in the mantle? Rev. Geophys. 32, 115–137.

Montagner, J.-P., 1998. Where can seismic anisotropy be detected in the Earth's mantel? In boundary layers. Pure Appl. Geophys. 151, 223–256.

Montagner, J.-P., Nataf, H.C., 1986. A simple method for inverting the azimuthal anisotropy of surface waves. J. Geophys. Res. 91, 511–520.

Montagner, J.-P., Tanimoto, T., 1991. Global upper mantle tomography of seismic velocities and anisotropies. J. Geophys. Res. 96, 20337–20351.

Mooney, W.D., Laske, G., Master, T.G., 1998. CRUST 5.1: a global crustal model at 5° × 5°. J. Geophys. Res. 103 (B1), 727–747.

Nicolas, A., Christensen, N.I., 1987. Formation of anisotropy in upper mantle peridotites—a review. In: Froidevaux, C., Fuchs, K. (Eds.), The Composition, Structure and Dynamics of the Lithosphere–Asthenosphere System, vol. 16. AGU Geophys. Ser., Washington, DC, pp. 111–123.

Pharaoh, T.C., 1999. Palaeozoic terranes and their lithospheric boundaries within the Trans-European Suture Zone (TESZ): a review. Tectonophysics 314, 17–41.

Plomerová, J., Šílený, J., Babuška, V., 1996. Joint interpretation of upper mantle anisotropy based on teleseismic P-travel time delays and inversion of shear-wave splitting parameters. Phys. Earth Planet. Inter. 95, 293–309.

Plomerová, J., Granet, M., Judenherc, S., Achauer, U., Babuška, V., Jedlička, P., Kouba, D., Vecsey, L., 2000. Temporary array data for studying seismic anisotropy of Variscan Massifs—the Armorican Massif, French Massif Central and Bohemian Massif. Stud. Geophys. Geod. 44, 195–209.

Plomerová, J., Arvidsson, R., Babuška, V., Granet, M., Kulhánek, O., Poupinet, G., Šílený, J., 2001. An array study of lithospheric structure across the Protogine zone, Varmland, south-central Sweden—signs of a paleocontinental collision. Tectonophysics 332, 1–21.

Poudjom Djomani, Y.H., O'Reilly, S.Y., Griffin, W.L., Morgan, P., 2001. Earth Planet. Sci. Lett. 184, 605–621.

Praus, O., Pěčová, J., Petr, V., Babuška, V., Plomerová, J., 1990. Magnetotelluric and seismological determination of the lithosphere–asthenosphere transition in Central Europe. Phys. Earth Planet. Inter. 60, 212–228.

Revenaugh, J.S., Jordan, T.H., 1991. Mantle layering from ScS reverberations. J. Geophys. Res. 96, 19763–19780.

Saltzer, R.L., Gaherty, J.B., Jordan, T.H., 2000. How are vertical shear wave splitting measurements affected by variations in the orientation of azimuthal anisotropy with depth? Geophys. J. Int. 141, 374–390.

Savage, M.K., 1999. Seismic anisotropy and mantle deformation: what have we learned from shear wave splitting? Rev. Geophys. 37, 65–106.

Šílený, J., Plomerová, J., 1996. Inversion of shear-wave splitting parameters to retrieve three-dimensional orientation of anisotropy in continental lithosphere. Phys. Earth Planet. Inter. 95, 277–292.

Silver, P.G., 1996. Seismic anisotropy beneath the continents: probing the depths of geology. Annu. Rev. Earth Planet. Sci. 24, 385–432.

Simons, F.J., Zielhuis, A., van der Hilst, R.D., 1999. The deep structure of the Australian continent from surface wave tomography. Lithos 48, 17–43.

Sobolev, S.V., Gressilaud, A., Cara, M., 1997. How robust is isotropic delay time tomography for anisotropic mantle. Geophys. Res. Lett. 26, 509–512.

van der Hilst, R.D., Kennett, B.L.N., Shibutani, T., 1998. Upper-mantle structure beneath Australia from portable array deployment. In: Braun, J., et al., (Eds.), Structure and Evolution of the Australian Continent, vol. 26. AGU Geodyn. Ser., Washington, DC, pp. 39–57.

Vauchez, A., Tommasi, A., Barruol, G., 1998. Rheological heterogeneity, mechanical anisotropy and deformation of the continental lithosphere. Tectonophysics 296, 61–86.

Wessel, P., Smith, W.H.F., 1995. The generic mapping tools (GMT) version 3.0. Technical references and cookbook. SOEST/NOAA.

Zandt, G., Ammon, Ch.J., 1995. Continental crust composition constrained by measurements of crustal Poisson's ratio. Nature 374, 152–154.

Zhang, Y.S., Tanimoto, T., 1993. High-resolution global upper mantle structure and plate tectonics. J. Geophys. Res. 98, 9793–9823.